Electronic Supplementary Material (ESI) for Sustainable Energy & Fuels.

Supporting Information

Hexagonal cluster Mn-MOF nanoflowers with super-wetting surface area for efficient and continuous solar-driven clean water production

Jiulong Wang,[a] Weike Wang,*[a] Xueyang Mu,[a] Zhengtong Li,[a] Chengbing Wang*[ab]

[a]School of Materials Science and Engineering, Shaanxi Key Laboratory of Green Preparation and Functionalization for Inorganic Material, Shaanxi University of Science & Technology, Xi'an, Shaanxi 710021, P. R. China.
[b]Zhejiang Wenzhou Research Institute of Light Industry, Wenzhou 325003, Zhejiang, China.

*Corresponding authors.

E-mail addresses: wangweike@sust.edu.cn, wangchengbing@gmail.com

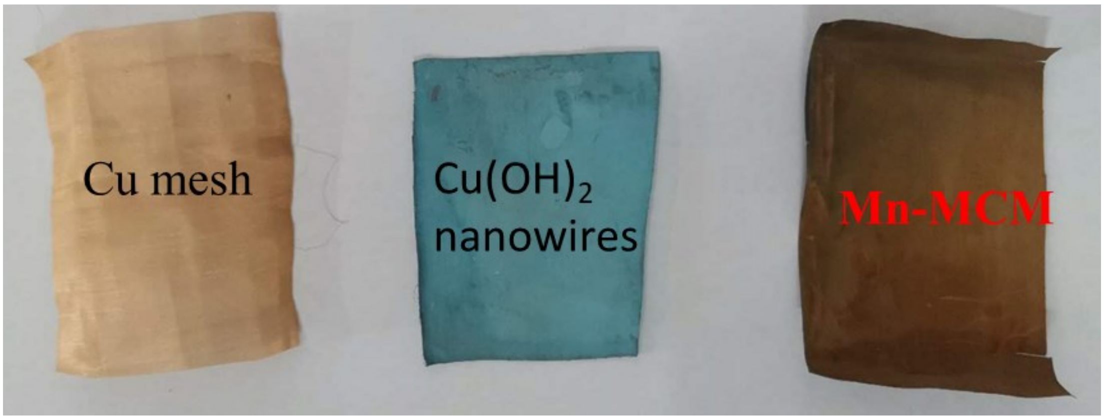

Fig. S1. The physical images of Mn-MCM being prepared.

The preparation of Mn-MCM is very simple and can be obtained in two steps, that is, growing copper hydroxide ($Cu(OH)_2$) nanowires on a copper mesh, and in the second step, growing Mn-dobdc on the $Cu(OH)_2$ nanowires by hydrothermally reaction, and finally obtaining the Mn-MCM.

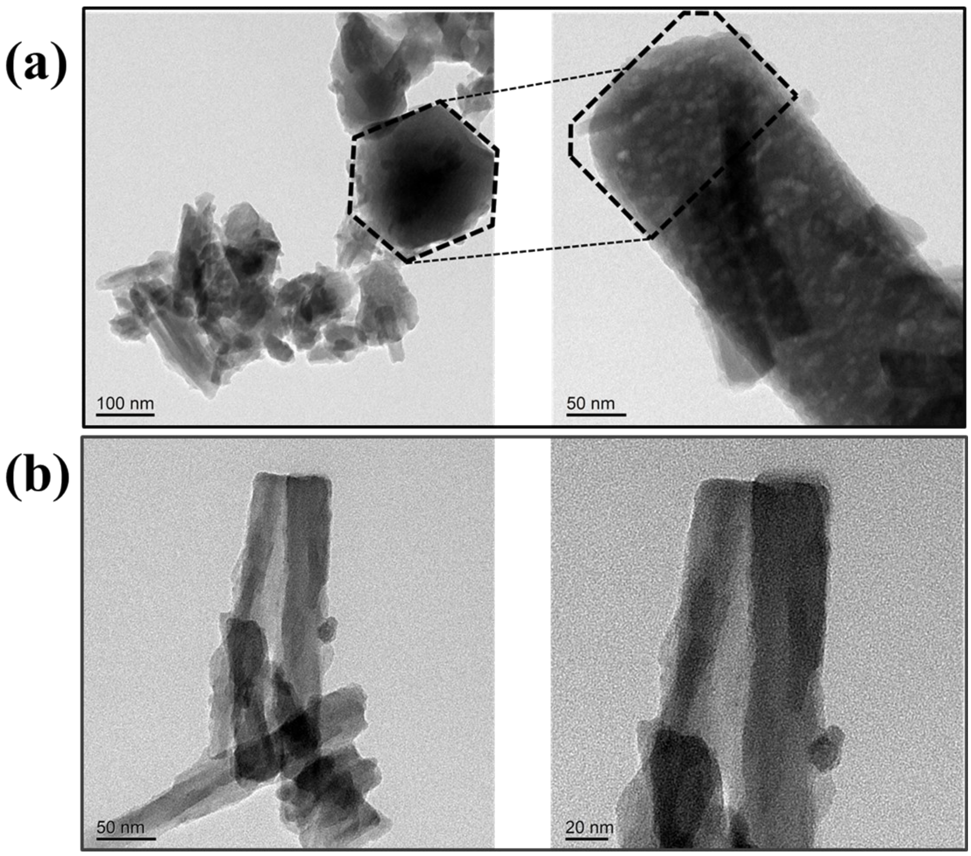

Fig. S2. TEM images of Mn-MCM. (a) Top-view and side-view TEM images of Mn-MCM with hexagonal prism structure at different magnifications. (b) TEM images of Mn-MCM with hexagonal prism cluster structure under different magnifications.

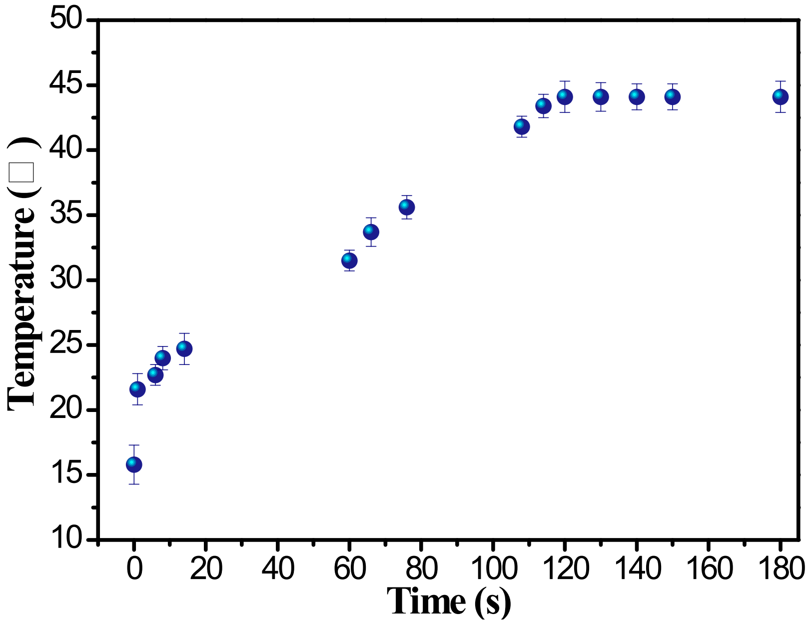

Fig. S3. The surface temperatures variation of Mn-MCM with time.

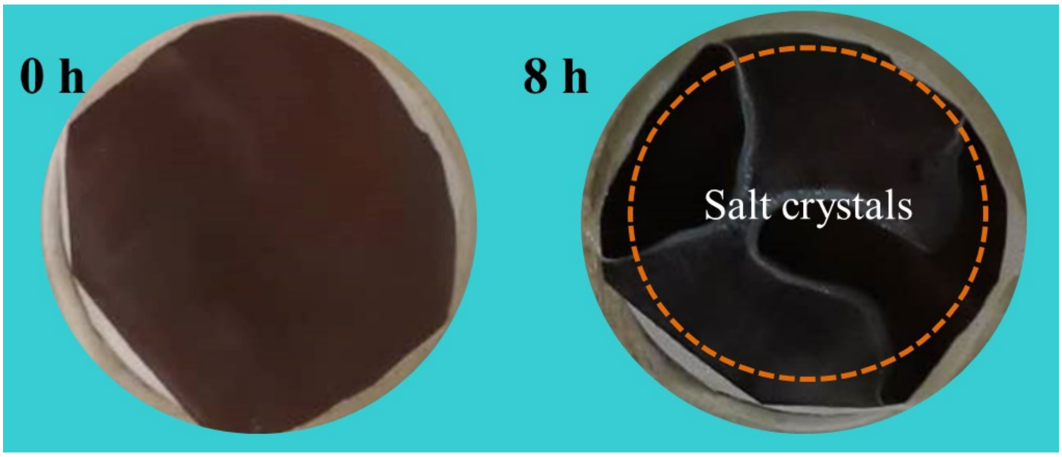

Fig. S4. The physical images before and after 8 h of the evaporation experiment of Mn-MCM.

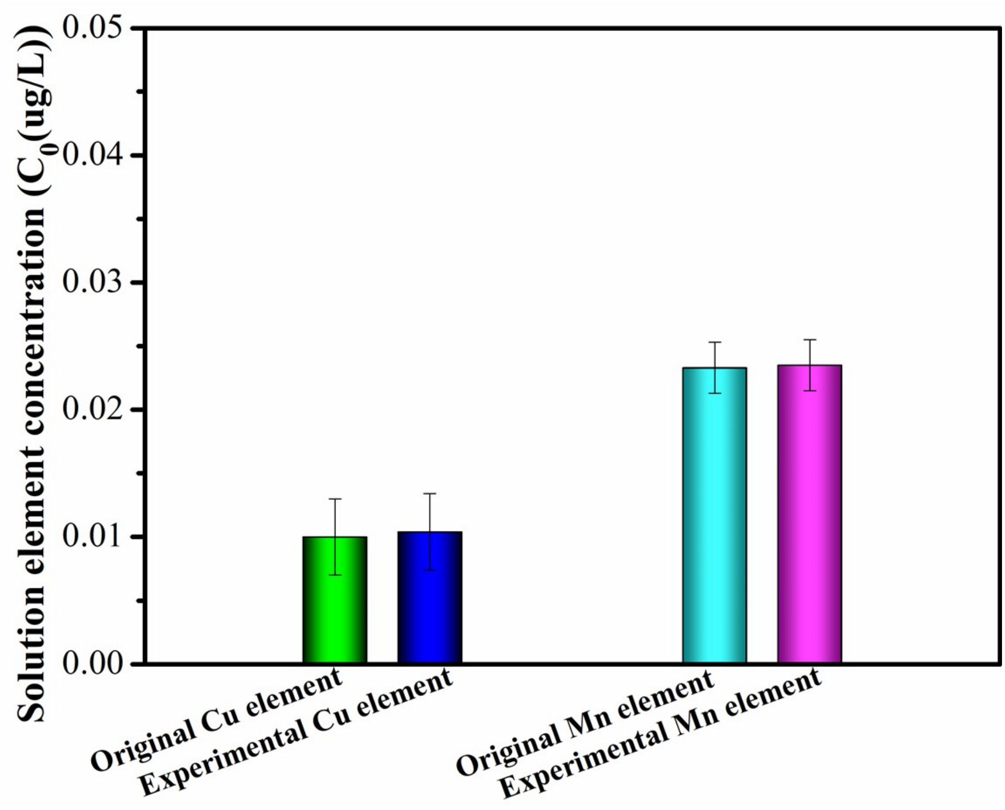

Fig. S5. The concentrations change of Cu element and Mn element in the solution (brine) before and after the evaporation experiment.

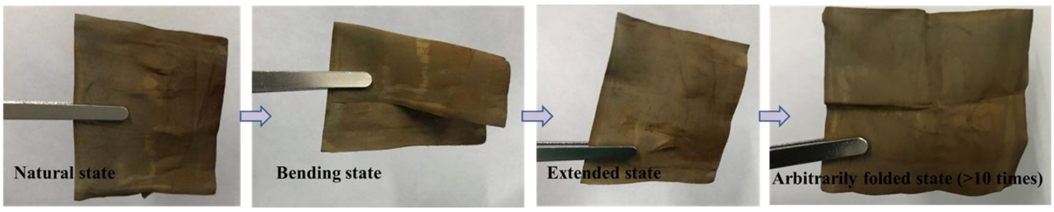

Fig. S6. The physical images of Mn-MCM before and after bending.

Fig. S7. The physical image of the experimental data acquisition instrument in the outdoor experiment.

Fig. S8. The fresh water collection device based on Mn-MCM under natural light.

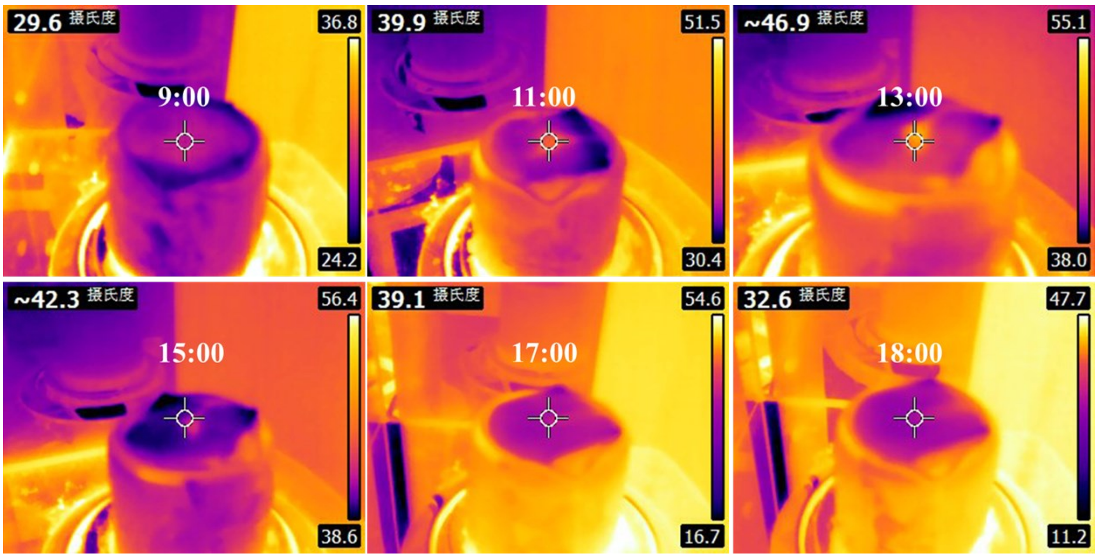

Fig. S9. The infrared images of the surface temperature of Mn-MCM with time under natural light.

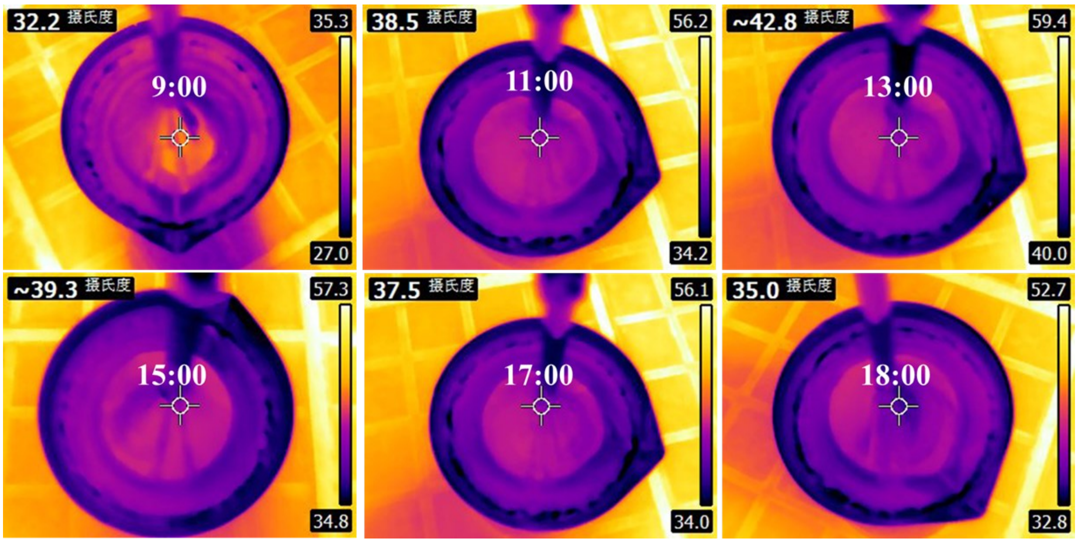

Fig. S10. Infrared camera images of the outdoor fresh water collection device under different time (Top view).

Section S1. Steady-state energy balance analysis:

The input heat flux (J_{in}) is 1 kW/m^2, and five main strategies for energy consumption are as follows: (1) water evaporation, (2) reflection and transmission energy loss, (3) conductive heat loss from the Mn-MCM to the water, (4) radiation heat loss from the Mn-MCM to the environment, and (5) convection heat loss from the Mn-MCM to the environment.

(1) Water evaporation consumption θ_1

The water evaporation consumption rate is equal to the evaporation efficiency; thus, θ_1 is about 81.5%

(2) Refection loss and transmission loss θ_2

Detected by UV spectrophotometer, the reflectance and transmittance of Mn-MCM are 12.51% and 1.15%; thus, the refection loss, θ_2 is 13.66%.

(3) Conduction loss θ_3

$$\theta_3 = (J_{cond} / J_{in}) \bullet (A_{evaporator} / A_{system})$$

The conductive heat flux from evaporator composed of Mn-MCM and polyvinyl chloride foam to water is calculated as $J_{cond} = k \cdot (\Delta T/L)$ (Fourier's law), k is the thermal conductivity of the evaporator (0.05 W m^{-1}K^{-1}), and $\Delta T/L$ is the gradient of temperature of Mn-MCM as measured by IR camera and thermocouple which is about 160 K/m. The picture (Fig. S11) illustrates the Mn-MCM surface area is major conductive path and the system area is absorbing the input solar energy. After several statistical calculations, $A_{evaporator}/A_{system}$ is about 0.77. Thus, we can calculate that θ_3 is about 0.6%.

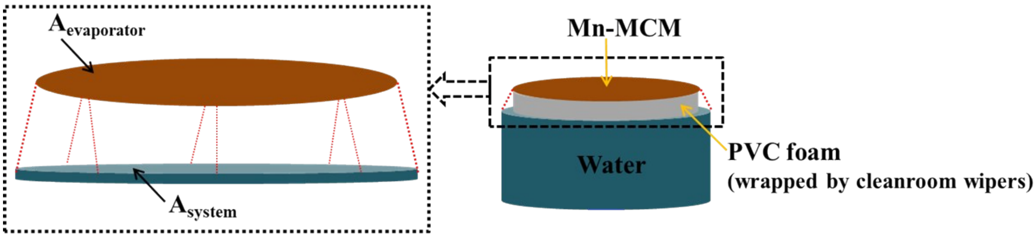

Fig. S11. The picture of evaporation system mode and fitting area for energy balance calculation.

(4) Radiation loss θ_4

$$\theta_4 = (J_{rad} / J_{in}) \cdot (A_{evaporator} / A_{system})$$

The radiation flux can be calculated by $J_{rad} = \varepsilon\, \sigma\, (T_1^4 - T_2^4)$ (Stefan-Boltzmann law), ε is the emissive rate which is calculated using an absorption spectrum and plank formula as 0.71, σ is the Stefan-Boltzmann constant (5.67×10^{-8} W m^{-2} K^{-4}), T_1 is the temperature of the absorber (the average surface temperature of Mn-MCM is about 309.75 K at 1 kw m^{-2}), T_2 is the ambient temperature (298.15 K). Thus, we can calculate that θ_4 is about 4.04%.

(5) Convection loss θ_5

$$\theta_5 = (P_{conv} / J_{in}) \cdot (A_{evaporator} / A_{system})$$

The convection heat loss can be calculated by $P_{conv} = h\, A_{surface}\, \Delta T$ (Newton's law of cooling), h is the convection heat transfer coefficient which can obtain by reference (5W m^{-2} K^{-1}) [1], the $A_{surface}$ is 0.00138474 m^2, the rest of the parameters remain the same as before. ($\Delta T = T_1 - T_2 = 11.6$ K). Thus, we can calculate that θ_4 is about 0.

In addition to these five main energy consumption parts (81.5% + 13.66% + 0.6% + 4.04% + 0%≈99.76%), the incoming solar energy may be dissipated by the test system or other ways.

Table S1 The evaporation performance of Mn-MCM was compared with other materials.

Materials	Evaporation rate ($kg\ m^{-2}\ h^{-1}$)	Evaporation Efficiency (%)	References
Mn-MOF-based copper mesh (Mn-MCM)	1.31 @ 1 sun	81.5% @ 1 sun	This paper
MDPC/SS mesh	1.222 @ 1 sun	84.3% @ 1 sun	[2]
Washable nonwoven photothermal cloth	1.24 @ 1 sun	83.1% @ 1 sun	[3]
2D Ti_3C_2 MXene membrane	1.31 @ 1 sun	71% @ 1 sun	[4]
Layer-by-layer 3D-printed evaporator	1.25 @ 1 sun	85.6% @ 1 sun	[5]
MoO_x HNS membrane	1.255 @ 1 sun	85.6% @ 1 sun	[6]
Polypyrrole coated cotton fabric	1.2 @ 1 sun	82.4% @ 1 sun	[7]
All-nanofiber aerogel	1.11@ 1 sun	76.3%@ 1 sun	[8]
Artificial tree with a reversed design	1.08@ 1 sun	74%@ 1 sun	[9]
Fe_3O_4@C film	1.07 @ 1 sun	67% @ 1 sun	[10]
CuS/PE membrane	1.021 @ 1 sun	63.9% @ 1 sun	[11]
Mxene/polyvinylidene fluoride	1@ 1 sun	84%@ 1 sun	[12]

References

[1] H. Ghasemi, G. Ni, A. M. Marconnet, J. Loomis, S. Yerci, N. Miljkovic, G. Chen, *Nat. Commun.*, 2014, **5**, 4449.

[2] S. N. Ma, W. Qarony, M. I. Hossain, C. T. Yipc, Y. H. Tsang, *Sol. Energy Mater. Sol. Cells*, 2019, **196**, 36-42.

[3] Y. Jin, J. Chang, Y. Shi, L. Shi, S. Hong, P. Wang, *J. Mater. Chem. A*, 2018, **6**, 7942-7949.

[4] J. Q. Zhao, Y. W. Yang, C. H. Yang, Y. P. Tian, Y. Han, J. Liu, X. T. Yin, W. X. Que, *J. Mater. Chem. A*, 2018, **6**, 16196-16204.

[5] Y. Li, T. Gao, Z. Yang, C. Chen, W. Luo, J. Song, E. Hitz, C. Jia, Y. Zhou, B. Liu, B. Yang, L. Hu, *Adv. Mater.*, 2017, **29**, 1700981.

[6] Q. C. Lu, Y. Yang, J. R. Feng, X. Wang, *Sol. RRL*, 2019, **3**, 1800277.

[7] D. D. Hao, Y. D. Yang, B. Xu, Z. S. Cai, *Appl. Therm. Eng*., 2018, **141**, 406-412.

[8] F. Jiang, H. Liu, Y. Li, Y. Kuang, X. Xu, C. Chen, H. Huang, C. Jia, X. Zhao, E. Hitz, Y. Zhou, R. Yang, L. Cui, L. Hu, *Acs Appl Mater Interfaces*, 2019, **9**, 1802158.

[9] H. Liu, C. Chen, G. Chen, Y. Kuang, X. Zhao, J. Song, C. Jia, X. Xu, E. Hitz, H. Xie, S. Wang, F. Jiang, T. Li, Y. Li, A. Gong, R. Yang, S. Das, L. Hu, *Adv. Energy Mater*., 2018, **8**, 1701616.

[10]R. Chen, K. H. Zhu, Q. M. Gan, Y. Q. Yu, T. Q. Zhang, X. W. Liu, M. M. Ye, Y. D.Yin, *Mater. Chem. Front*., 2017, **1,** 2620-2626.

[11]M. Y. Shang, N. Li, S. D. Zhang, T. T. Zhao, C. Zhang, C. Liu, H. F. Li, Z. Y. Wang, *ACS Appl. Energy Mater*, 2017, **1**, 56-61.

[12] R. Li, L. Zhang, L. Shi, P. Wang, *ACS Nano.*, 2017, **11**, 3752.